Experimental investigation of the penetration of a high-velocity gas jet through a liquid surface

By ROBERT B. BANKS
SEATO Graduate School of Engineering, Bangkok, Thailand

AND D. V. CHANDRASEKHARA
Technological Institute, Northwestern University, Evanston, Illinois

(Received 21 June 1962)

This investigation is concerned with the phenomenon of a gas jet impinging on and penetrating into a liquid. The study has been restricted to the cases of circular and plane jets penetrating a liquid at right angles. Both 'free streamline' and turbulent jets were considered. The phenomenon was analysed from two viewpoints. The first, a stagnation-pressure analysis, related the depth of the surface depression or cavity to the stagnation pressure based on the centre-line velocity of the jet in the neighbourhood of the surface. The second, a displaced-liquid analysis, related the weight of the liquid displaced from the cavity to the momentum of the jet.

Numerous experiments were conducted in which the cavity depth, diameter or width, and peripheral lip height were measured. The role of surface tension in affecting the cavity depth was considered and the phenomenon of drop formation was examined. Some attention was given to the case of a plane jet impinging on a moving liquid. It was found that the experimental data fit into the framework of these analyses quite consistently.

1. Introduction

Numerous studies have been carried out recently on topics concerned with the fluid mechanics of jets in the proximity of rigid boundaries. These investigations have been devoted primarily to determination of velocity and pressure distributions for various configurations. A logical extension of such studies is to examine similar problems when a jet is impinging on a deformable surface such as a liquid. The simplest cases to consider are the circular and plane jet impinging normally on a liquid surface as shown in figure 1. Depending on the relative distance of the nozzle above the surface, the gas jet will behave as a 'free streamline' (i.e. irrotational with sharp boundaries) flow or as a turbulent spreading jet. Hence four categories of problems are presented, depending on whether the jet is circular or plane and whether it is to be considered a potential or a turbulent flow. The velocity of the jet is V_J at the nozzle and the diameter or width of the nozzle is d_0 or b_0, respectively. The exit plane of the nozzle is a distance H above the still liquid surface. Fluid properties are indicated in the figure.

The impinging jet causes a depression on the liquid surface, though in the case of a strong jet it is more descriptive to say that the penetrating jet creates a cavity in the liquid. The maximum depth of the depression or cavity is n_0. When the depression is relatively large, a lip, of height n_p, is formed around or along the cavity. This lip defines a cavity diameter, d_c, or width, b_c. In addition, other features are observed. The cavity bottom tends to oscillate vertically and the sides laterally in the case of deep cavities. There is considerable gas entrainment in the liquid. Surface ripples are propagated from the disturbed zone. A circulation is induced in the liquid as a result of the tangential drag of the gas on the liquid. Under certain conditions, liquid drops are formed and projected from the region of the cavity.

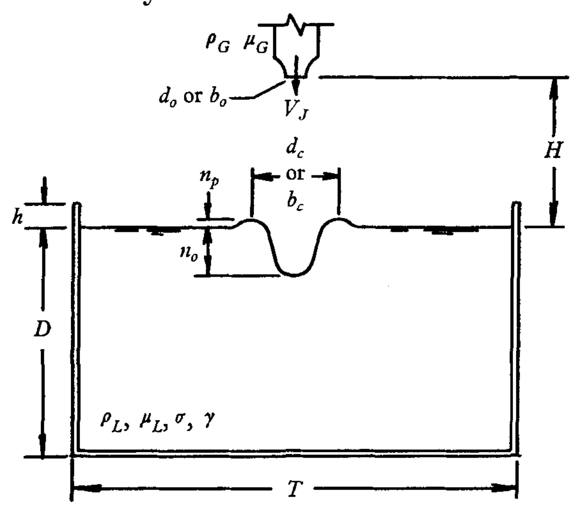

FIGURE 1. Definition sketch for the jet penetration study.

The aim of this experimental investigation was to determine the cavity depth, diameter or width, and lip height as functions of the various independent variables. The aspect of liquid-drop formation was studied to a limited extent. Some consideration was given to the case in which the liquid was moving horizontally with respect to a vertical plane jet. Features of cavity oscillation, ripple formation, and circulation in the liquid were not studied in detail. In all of the experiments, air was the gas and water was the liquid.

2. Flow fields associated with impinging and penetrating jets

2.1. *The 'free-streamline' jet*

One approach to the problem is to consider a free-streamline jet impinging normally on a rigid flat surface. The solution to the plane jet problem has been presented by Milne-Thompson (1960) who gives the following expression for the potential-flow velocity distribution along the surface

$$y/b_0 = 2/\pi\{\arctan(u/V_J) + \operatorname{arctanh}(u/V_J)\}. \tag{2.1}$$

This relationship is shown in figure 2. It is seen that the velocity along the surface is essentially equal to the approach velocity at a distance of about two nozzle widths from the stagnation point. The pressure distribution shown in figure 2 was obtained from the Bernoulli equation. The thrust on the surface is obtained from elementary momentum considerations, i.e.

$$R = \rho_G b_0 V_J^2 = 2\int_0^\infty p\,dy, \tag{2.2}$$

where ρ_G is the density of the gas. The form of (2.1) does not permit an explicit expression for the pressure distribution. Since an explicit form was necessary to proceed with the analysis, a normal curve was selected as an approximation to the exact pressure distribution. If it is assumed that

$$p/\tfrac{1}{2}\rho_G V_J^2 = \exp\{-\alpha(y/b_0)^2\} \tag{2.3}$$

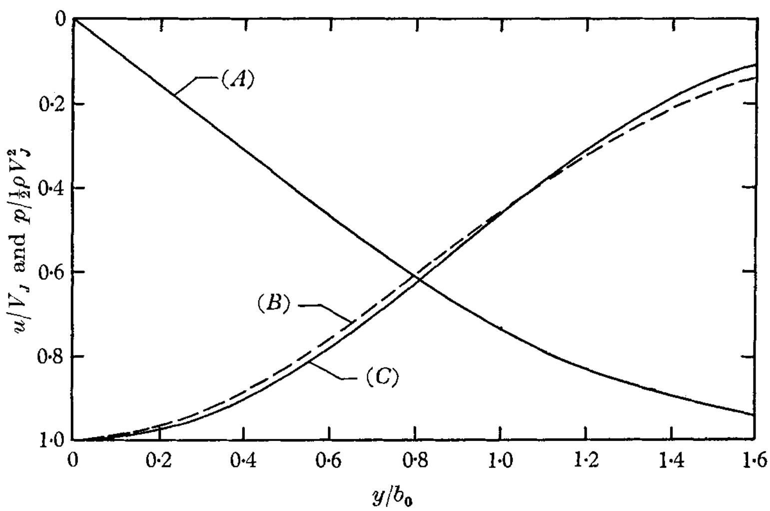

FIGURE 2. Velocity and pressure distribution of a plane free jet impinging on a flat surface. Comparison of assumed normal distribution with exact pressure distribution.
$(A)\ \dfrac{y}{b_0} = \dfrac{2}{\pi}\left(\arctan\dfrac{u}{V_J} + \operatorname{arctanh}\dfrac{u}{V_J}\right)$; $(B)\ \dfrac{p}{\frac{1}{2}\rho V_J^2} = \exp\left\{-\dfrac{\pi}{4}\left(\dfrac{y}{b_0}\right)^2\right\}$; $(C)\ \dfrac{p}{\frac{1}{2}\rho V_J^2} = 1 - \left(\dfrac{u}{V_J}\right)^2$.

then from (2.2) it is established that $\alpha = \frac{1}{4}\pi$. This approximation is shown in figure 2.

A similar expression may be obtained for the case of a circular jet. Though it is not possible to obtain an exact solution, corresponding to (2.1), experimental data indicate that an error curve approximation is not unreasonable. For the circular case, the thrust on the surface is

$$R = \tfrac{1}{4}\rho_G \pi d_0^2 V_J^2 = 2\pi\int_0^\infty pr\,dr, \tag{2.4}$$

and if the pressure distribution is assumed to be

$$p/\tfrac{1}{2}\rho_G V_J^2 = \exp\{-\beta(r/d_0)^2\}, \tag{2.5}$$

then a value of $\beta = 2$ is obtained from (2.4). Figure 3 compares data obtained by Gibson (1934) with the assumed distribution.

Equations (2.3) and (2.5) are employed below to describe the pressure distribution on a liquid surface, for the case of a weak jet, when the nozzle is close to the surface, i.e. for small values of H/d_0 or H/b_0. In this instance the jet has not yet begun to spread and hence may be regarded as a potential flow.

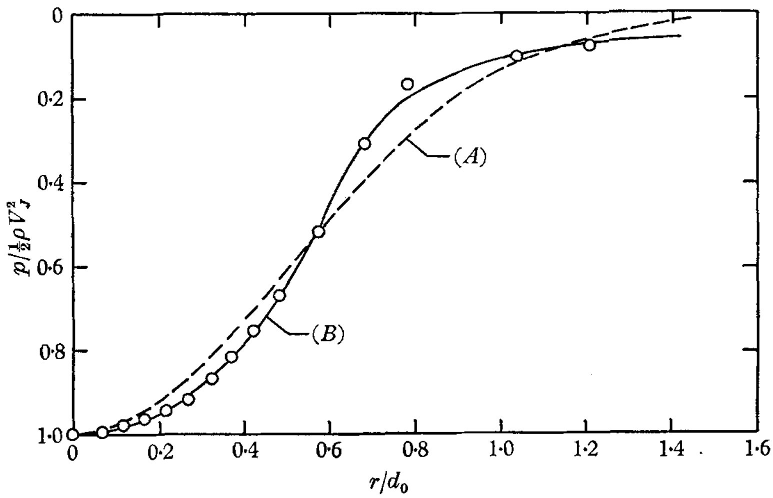

FIGURE 3. Pressure distribution of a circular free jet impinging on a flat surface. Comparison of assumed normal distribution with data of Gibson (1934).

(*A*) $p/\frac{1}{2}\rho V_J^2 = \exp\{-2(r/d_0)^2\}$; (*B*) data of Gibson (1934).

2.2. *The free turbulent jet*

For large values of H/d_0 or H/b_0, the jet velocity is reduced as a result of spreading. The value of the centre-line velocity in the neighbourhood of the surface may be estimated from the equation for the velocity distribution of a free turbulent jet. For the plane case

$$V_0/V_J = K_1(b_0/x)^{\frac{1}{2}}, \tag{2.6}$$

where V_0 is the centre-plane velocity. The complete velocity distribution of a plane jet has been expressed in numerous forms. Some investigators, e.g. Albertson, Dai, Jensen & Rouse (1950), Forstall & Gaylord (1955) and Miller & Comings (1957), have established that a normal error curve is descriptive of the distribution, i.e.

$$\frac{V}{V_0} = \exp\left\{-\frac{1}{2C_1^2}\left(\frac{y}{x}\right)^2\right\}, \tag{2.7}$$

where V is the velocity at (x, y).

The region of fully developed turbulent flow begins some distance downstream from the plane of the nozzle. A transition zone exists for several nozzle widths in which the uniformly distributed velocity at the nozzle acquires its fully developed form. The length of this zone, x_0, is expressed by $x_0 = n_1 b_0$. Previous investigations have established values of the constants K_1 and n_1; some results are given in table 1.

Similar expressions apply to the circular turbulent jet. The centre-line velocity, V_0, is given by

$$V_0/V_J = K_2 d_0/x, \tag{2.8}$$

and presumably the complete velocity distribution, $V = V(x, r)$, may be expressed by a normal curve

$$\frac{V}{V_0} = \exp\left\{-\frac{1}{2C_2^2}\left(\frac{r}{x}\right)^2\right\}. \tag{2.9}$$

The length of the potential core is $x_0 = n_2 x$. Values of K_2 and n_2 obtained in previous studies are given in table 2.

Investigator	K_1	n_1
Albertson *et al.* (1950)	2·28	5·2
Miller & Comings (1957)	2·63	7·0
Reichardt (1941)	2·40	—

TABLE 1. Constants for the plane turbulent jet.

Investigator	K_2	n_2
Albertson *et al.* (1950)	6·2	6·2
Poreh & Cermak (1959)	7·7	9·0
Forstall & Gaylord (1955)	6·4	5·0
Corrsin & Uberoi (1949)	6·6	—
Folsom & Ferguson (1949)	5·13	8·0
Hinze & Van der Hegge Zijnen (1948)	6·39	10·0

TABLE 2. Constants for the circular turbulent jet.

3. Analytical models of the penetrating jet

3.1. *Dimensional analysis*

For the purpose of dimensional analysis, the momentum of the jet, $M = \rho_G a_0 V_J^2$, is taken as an independent variable. The area, a_0, is $\frac{1}{4}\pi d_0^2$ for the circular jet and $b_0 L$ for the plane jet; L is the length of the plane nozzle. Neglecting the effects of viscosity and surface tension, dimensional analysis yields the following expression for the circular case

$$M/\gamma n_0^3 = f_1(n_0/H, H/d_0), \tag{3.1}$$

where $\gamma = \rho_L g$ is the specific weight of the liquid. For the plane case the corresponding expression is

$$M/\gamma L n_0^2 = f_2(n_0/H, H/b_0). \tag{3.2}$$

Other combinations of linear dimensions could appear as volume units in the denominators of the left-hand members of (3.1) and (3.2). For example,

$$M/\gamma n_0 H^2 = f_3(n_0/H, H/d_0) \tag{3.3}$$

is an alternative expression for the circular jet and

$$M/\gamma L n_0 H = f_4(n_0/H, H/b_0) \tag{3.4}$$

for the plane jet. If a Froude number is defined as $F = V_J^2/gn_0$, the left-hand members of the preceding four equations become products of a density ratio, a length or area ratio, and the Froude number. For example, the left-hand side of (3.4) becomes $(\rho_G/\rho_L)(b_0/H)F$. If a modified Froude number is termed $F_* = (\rho_G/\rho_L)F$, then (3.4) becomes

$$F_* = f_4^*(n_0/H, H/b_0), \tag{3.5}$$

and the other expressions could be presented the same way. It is not surprising to see that a Froude number plays a predominant role in the phenomenon.

3.2. *Analytical model I: stagnation pressure analysis*

Let V_s denote the centre-line velocity of the jet in the proximity of the stagnation point. Neglecting the effect of surface tension, it is assumed that

$$\tfrac{1}{2}\rho_G V_s^2 = \gamma n_0, \tag{3.6}$$

where n_0 is the maximum depth of the depression or cavity in the liquid. For the circular free-streamline jet, V_s is equal to V_J, and one obtains

$$M/\gamma n_0 d_0^2 = \tfrac{1}{2}\pi. \tag{3.7}$$

The corresponding expression for the plane free-streamline jet is

$$M/\gamma L n_0 b_0 = 2. \tag{3.8}$$

In the case of a turbulent jet, V_s is less than V_J as a result of spreading. For the circular case, (2.8) is employed to estimate the value of V_s; the nozzle height, H, is arbitrarily selected as the value of x. This yields

$$M/\gamma n_0 H^2 = \pi/2K_2^2. \tag{3.9}$$

A similar consideration for the plane turbulent jet, using (2.6) to estimate the centre-plane velocity near the stagnation point, gives

$$M/\gamma L n_0 H = 2/K_1^2. \tag{3.10}$$

3.3. *Analytical model II: displaced liquid analysis*

The displaced liquid analysis assumes that the force which the jet exerts on the liquid is equal to the weight of the displaced liquid. It is also assumed that the depression is sufficiently small that the change in shape of the liquid surface does not appreciably alter the velocity and pressure distributions of the gas flow. This implies that the vertical component of momentum of the departing gas flow is zero. To determine the weight of the displaced liquid, it is assumed that the cavity profile is established by a known pressure distribution on the surface.

For the circular free-streamline jet, using the pressure distribution of (2.5) to compute the weight of displaced liquid, one obtains

$$M/\gamma n_0 d_0^2 = \pi/\beta. \tag{3.11}$$

This result, when compared with (3.7), reiterates that $\beta = 2$. The plane free-streamline case, using (2.3) as the pressure distribution, results in

$$M/\gamma L n_0 b_0 = (\pi/\alpha)^{\frac{1}{2}}, \tag{3.12}$$

and it is noticed from (3.8) that this implies again that $\alpha = \frac{1}{4}\pi$.

Next, the results of a study by Poreh & Cermak (1959) are employed to examine the case of the circular turbulent jet impinging on a liquid surface. These investigators measured the pressure distribution on a submerged rigid flat surface caused by a submerged liquid jet. They obtained the expression

$$n = (M/\gamma H^2)\{38{\cdot}5 - 4800(r/H)^2\}, \tag{3.13}$$

where n, in their terminology, is the additional pressure head on the solid boundary due to the normally impinging jet. It is now assumed that this quantity, $n = n(r)$, is the profile of a liquid surface resulting from an impinging circular gas jet. Equation (3.13) may be rewritten in the form

$$n/n_0 = 1 - \beta_*(r/H)^2, \tag{3.14}$$

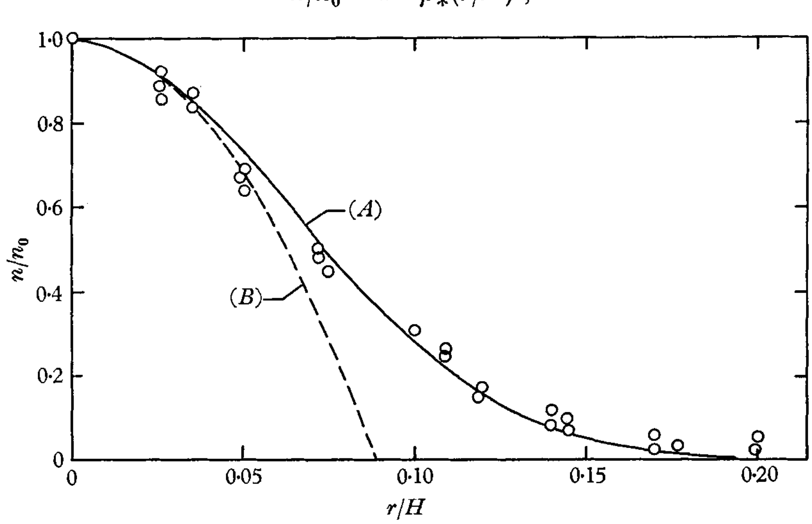

FIGURE 4. Pressure distribution of a circular turbulent jet impinging on a flat surface. Comparison of assumed normal distribution with data of Poreh & Cermak (1959). (A) $n/n_0 = \exp\{-\beta_*(r/H)^2\}$; (B) $n/n_0 = 1-\beta_*(r/H)^2$. ○, Data of Poreh & Cermak (1959) $\beta_* = 125$.

where $\beta_* = 4800/38{\cdot}5 = 125$ and $n_0 = 38{\cdot}5M/\gamma H^2$. The experimental results of Poreh & Cermak and (3.14) are shown in figure 4. In an effort to describe these data over a broader range a normal error curve was fitted. It is observed in figure 4 that such a curve, viz.

$$n/n_0 = \exp\{-\beta_*(r/H)^2\} \tag{3.15}$$

agrees fairly well with the data. This assumed profile equation enables one to compute the volume of the cavity. Equating the thrust of the jet to the weight of displaced liquid gives

$$M/\gamma n_0 H^2 = \pi/\beta_*, \tag{3.16}$$

which may be expressed in the alternative form

$$n_0/H = (\pi/\beta_*)^{\frac{1}{2}}/(M/\gamma n_0^3)^{\frac{1}{2}}. \tag{3.17}$$

Comparison of (3.9) and (3.16) reveals the interesting relationship, $\beta_* = 2K_2^2$. Also, (2.5) and (3.15) indicate that the same pressure distribution and hence cavity profile will be produced by the circular free-streamline jet and the turbulent jet when

$$\beta_*/\beta = (H/d_0)^2. \tag{3.18}$$

A similar analysis is proposed for the case of the plane turbulent jet. It is assumed that a normal error curve, analogous to (3.15), is descriptive of the cavity shape, i.e.

$$n/n_0 = \exp\{-\alpha_*(y/H)^2\}. \tag{3.19}$$

This assumption results in

$$M/\gamma L n_0 H = (\pi/\alpha_*)^{\frac{1}{2}}, \tag{3.20}$$

or, alternatively,

$$n_0/H = (\pi/\alpha_*)^{\frac{1}{2}}/(M/\gamma L n_0^2). \tag{3.21}$$

Again, a relationship is established by (3.10) and (3.20), which gives $\alpha_* = \frac{1}{4}\pi K_1^4$. Finally, with regard to (2.3) and (3.19), the same liquid surface profile is obtained for the plane free-streamline jet and turbulent jet when

$$\alpha_*/\alpha = (H/b_0)^2. \tag{3.22}$$

3.4. *Effect of surface tension*

The above analysis may be extended to take into account the effect of surface tension. To accomplish this most easily, it is assumed that the cavity shape is still described by a normal error curve, i.e. by (3.15) and (3.19) for the turbulent jet, and by expressions corresponding to (2.3) and (2.5) for the free-streamline jet. For the circular case, the condition for stagnation-point equilibrium is

$$\tfrac{1}{2}\rho_G V_s^2 = \gamma n_0 + 2\sigma/R_0 \tag{3.23}$$

instead of (3.6); σ is the surface tension. The radius of curvature at the stagnation point, R_0, is determined from (3.15); the result is $R_0 = H^2/2\beta_* n_0$. Substituting this quantity in (3.23) and again using (2.8) to estimate V_s, one obtains

$$M/\gamma n_0 H^2 = (\pi/2K_2^2)(1 + 4\sigma\beta_*/\gamma H^2). \tag{3.24}$$

If the second term in the brackets of (3.24) is large with respect to unity, i.e. if surface tension dominates the gravity body force, then (3.24) reduces to $M = \text{const.}\,(\sigma n_0)$. A similar result is obtained for the free-streamline case.

3.5. *Deep cavities*

The normal error curve serves as a convenient description of the pressure distribution and for very shallow cavities it would appear to be a reasonably accurate expression of the cavity shape. However, for cavities of moderate or considerable depth, the above analytical models need to be modified or replaced.

The simplest modification, and one which accurately predicts a trend of the deep-cavity data, is the following. When a cavity of appreciable depth is formed, the jet travels somewhat farther than it would otherwise and hence the velocity near the stagnation point is reduced due to further spreading. This 'added travel of jet' modification is manifested by substituting $H + n_0$, instead of H, in the expressions for the centre-line velocity distributions, (2.6) and (2.8), employed in the stagnation-pressure analysis. Alternatively, it is apparent that as the cavity becomes deeper, the assumption that the velocity and pressure distributions in the gas flow field are unaffected is no longer valid. Such alteration in pressure distribution, in turn, changes the cavity shape. A rather arbitrary way to alter and 'deepen' the cavity, but with an eye on the above, is to replace H by $H+n_0$ in the equations for the cavity profile (3.15) and (3.19), as used in the displaced-liquid analysis. From either viewpoint, this modification leads to the same result. Neglecting the effect of surface tension, the equation for the circular turbulent jet case becomes

$$\frac{n_0}{H} = \frac{(\pi/\beta_*)^{\frac{1}{2}}}{(M/\gamma n_0^3)^{\frac{1}{2}} - (\pi/\beta_*)^{\frac{1}{2}}}, \tag{3.25}$$

and for the plane jet case one obtains

$$\frac{n_0}{H} = \frac{(\pi/\alpha_*)^{\frac{1}{2}}}{(M/\gamma L n_0^2) - (\pi/\alpha_*)^{\frac{1}{2}}}. \tag{3.26}$$

These relationships are modifications of (3.17) and (3.21), respectively.

Completely rational models of the deep cavity would require a precise formulation of the mechanics of interaction between the liquid and the gas. Birkhoff (1950) has presented a hodograph method for the determination of the stationary streamline of discontinuity in an infinite-cavity flow; such a streamline would correspond closely to the gas–liquid interface of the present problem. Birkhoff & Zarantonello (1957) have outlined various approximate solutions to axially-symmetrical flow problems which bear on the jet-penetration phenomenon. One such solution involves the construction of Rankine-type flows. This approach utilizes a half-line of sources of constant density as an approximation to an infinite-cavity flow. The result anticipates a paraboloidal cavity whose shape, in the present nomenclature, is $r^2 = 4m(n+m)$, where m is the source strength. Intuitively, cavities of approximately elliptical shape would be formed when the jet is deeply penetrating. However, it appears that knowledge of the exact shape of the cavity is not vital as far as the prediction of the cavity depth is concerned. A more important feature in this respect is that the vertical component of momentum of the departing gas flow is appreciable when the ratio of cavity diameter (or width) to depth becomes small.

4. Laboratory apparatus and experimental procedure

4.1. *Apparatus*

Three separate laboratory arrangements were assembled for the purpose of obtaining experimental data. These are described as follows.

(*a*) *Deep water tank with circular nozzles.* A Plexiglass tank of 30 in. diameter and 42 in. height was employed to study the behaviour of an air jet penetrating into deep water. The tank rested on a steel frame; vertical extension of the frame supported the air inlet pipe and nozzle. The latter was situated so that the air flow was vertically downward and on the tank centre-line. The distance between the still water surface and the plane of the nozzle was altered by changing either the depth of water in the tank or by altering the length of a pipe section upstream from the nozzle. The nozzles employed in the deep water experiments were of three sizes: $\frac{1}{4}$, $\frac{1}{2}$ and $\frac{3}{4}$ in. diameter. They were designed in accordance with ASME specifications for elliptical-approach nozzles. The pipe to which the nozzles were attached was $1\frac{1}{2}$ in. in diameter. Air was supplied by a Roots–Connerville positive displacement blower.

(*b*) *Shallow water tank with circular nozzles.* A Plexiglass tank, approximately 28 in. square with sides about 3 in. in height, was used for experiments on jet penetration in shallow water. The three nozzles were connected to an inlet pipe of $1\frac{1}{2}$ in. diameter such that the nozzle centre-line passed through the centre of the tank.

(*c*) *Rectangular channel with plane nozzle.* Jet penetration experiments involving plane nozzles were conducted in an open channel of 12 in. width, 18 in. height and 18 ft. length. The sides and horizontal bottom of the channel were made of Plexiglass and were supported by a frame made of steel angles and pipe. Air was supplied to a brass manifold installed between the vertical side-walls of the channel. A horizontal baffle plate, built inside the manifold, produced a uniform distribution of flow from the plane nozzle. The width of the nozzle could be varied by means of two narrow bars installed in guide slots at the channel walls. Moulding clay was placed around the manifold sides to prevent leakage of air. The depth of water in the channel could be easily altered to change the effective nozzle height. A small centrifugal pump was employed to recirculate the water through the channel when desired.

4.2. *Metering*

Mass flow rates for the circular-jet studies were determined by employing the test nozzles as flow meters. Flow rates for the plane-nozzle experiments were obtained by means of a sharp-edged orifice plate installed in the air supply pipe. Flow rates were varied, in both the circular and plane nozzle tests, by means of a small gate valve installed at a pipe-tee in the air supply pipe between the blower and the respective meter, i.e. a portion of the flow was discharged to atmosphere. Flow rates were computed from the customary formulas for compressible flow metering. Water which was recirculated through the open channel during some of the plane-jet experiments was metered by a sharp-edged orifice plate.

4.3. *Experimental procedure*

A typical experiment was conducted as follows. The test nozzle was set at a desired height above the water surface and the gate valve, by-passing the air flow from the blower, was slowly closed until a shallow cavity appeared on the water surface. A hook gauge, whose zero reading had been established previously by the still water surface, was used to measure the cavity depth. This apparatus was designed with a horizontal arm sufficiently long to probe the cavity from below without disturbing the air-flow pattern or the cavity profile. Other probes were used to measure the cavity diameter or width and the height of the peripheral lip. In nearly all experiments, the cavity bottom oscillated to some degree. Measurements were made of the maximum and minimum cavity depths for each experiment, and the arithmetical average was used in all computations. Subsequent experiments were conducted by increasing the air flow rate and repeating the measurement procedure.

4.4. *Scope of experiments*

A total of 282 experiments were conducted; 69 were carried out in the deep water tank, 110 in the shallow water tank, and 103 in the rectangular channel. The ranges of test variables were as follows:

Nozzle diameter, d_0:	$\frac{1}{4}$, $\frac{1}{2}$, $\frac{3}{4}$ in.
Nozzle width, b_0:	$\frac{1}{16}$ in.
Nozzle elevation, H:	0·10 to 1·0 ft.
Water depth, D:	0·083 to 3·0 ft.
Nozzle velocity, V_J:	25·2 to 420 ft./sec.
Volumetric flow rate, Q:	0·0086 to 1·158 ft.^{3}/sec (STP).
Nozzle Reynolds number, R_J:	2150 to 80,000.
Moving-water velocity, V_L:	0·175 to 0·551 ft./sec.
Moving-water Froude number, F_L:	0·040 to 0·238.

$H = 0{\cdot}7$ in., $b_0 = \frac{1}{16}$ in., $L = 1{\cdot}5$ in., $H/b_0 = 10{\cdot}7$

Photo. no.	V_J (ft./sec)	n_0 (in.)	M (lb.)	$M/\gamma L n_0^2$	n_0/H
134	45	0·24	0·0031	1·02	0·35
133	63	0·39	0·0061	0·72	0·59
132	79	0·51	0·0095	0·67	0·77
131	96	0·67	0·0141	0·58	1·00
130	121	0·87	0·022	0·54	1·30
129	161	1·22	0·040	0·49	1·82
128	179	1·34	0·049	0·50	2·0

TABLE 3. Test variables of figure 5, plate 1.

$V_J = 178$ ft./sec, $b_0 = \frac{1}{16}$ in., $L = 1{\cdot}5$ in., $M = 0{\cdot}0486$ lb.

Photo. no.	H (in.)	n_0 (in.)	H/b_0	$M/\gamma L n_0^2$	n_0/H
102	0	1·8	0	0·29	∞
103	0·2	1·7	3·15	0·32	8·6
105	0·4	1·5	6·3	0·42	3·7
106	0·8	1·3	12·6	0·50	1·7
108	1·4	1·2	22·1	0·60	0·89
110	2·2	1·1	34·7	0·80	0·49
113	3·2	0·7	50·4	1·80	0·23

TABLE 4. Test variables of figure 6, plate 2.

4.5. *Photographs*

None of the three laboratory arrangements described above proved suitable for photography and so a special series of tests was carried out. This series was conducted in an open channel of 6 ft. length and 2 ft. height. The vertical side-walls of the channel were made of glass and were $1\frac{1}{2}$ in. apart. Water could be circulated through the channel or kept quiescent at any depth up to 20 in. A variable-throat plane nozzle was constructed for this series. The nozzle width could be varied from zero to $\frac{1}{8}$ in.; the length of the slot was $1\frac{1}{2}$ in. To minimize air leakage, grease was applied to the sides of the nozzle assembly, and the latter was attached to a point gauge to permit convenient changes in nozzle elevation. When the nozzle was at the desired height, a C-clamp was used to draw two steel angles at the top of the channel closer together; this assured a tight fit between the nozzle assembly and the glass side-walls. The nozzle approach consisted of two $\frac{1}{2}$ in. radius quarter-cylinders attached to two $\frac{1}{8}$ in. thick brass straps. The latter were clamped to a head piece which also served as a connexion to the air supply line. A machine bolt passing through the nozzle chamber could be turned and tightened to give the desired nozzle opening. A $\frac{1}{16}$ in. diameter hole was drilled through one of the brass straps at the stagnation point defined by the $\frac{1}{2}$ in. radius brass cylinder. A tube leading to a manometer column was attached to this hole; by this means, the air-flow rate could be determined. Photographs of two series of experiments are shown in figures 5 and 6, plates 1 and 2. Tables 3 and 4 give the various test variables for these figures.

5. Experimental results

5.1. *Circular jet cavities*

Data obtained in the deep water tank using circular nozzles are shown in figure 7. All three nozzles were tested at values of $H = 0{\cdot}25$, $0{\cdot}50$, $0{\cdot}75$ and $1{\cdot}0$ ft. Data obtained in the shallow water tank with the same nozzles are presented in figure 8.

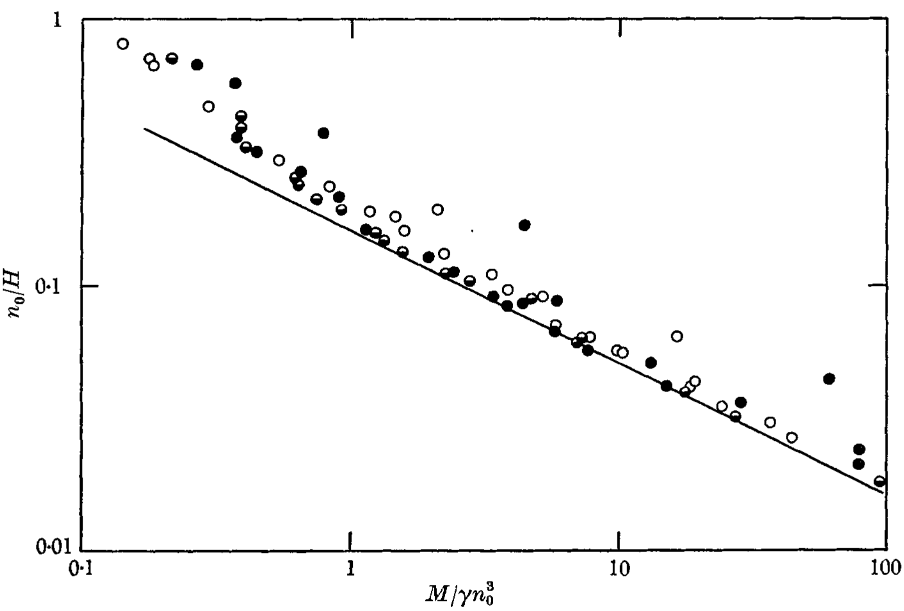

FIGURE 7. Cavity-depth data obtained in the deep-water test apparatus using circular nozzles. Nozzle diameter: ○, $\frac{1}{4}$ in.; ⊖, $\frac{1}{2}$ in.; ●, $\frac{3}{4}$ in.

All of the circular jet data, i.e. the data of figures 7 and 8, are shown in figure 9. The equation of the line passing through the plotted points of figure 9 is given by (3.25) with a value of $\beta_* = 125$. The bend in the upper part of the curve is

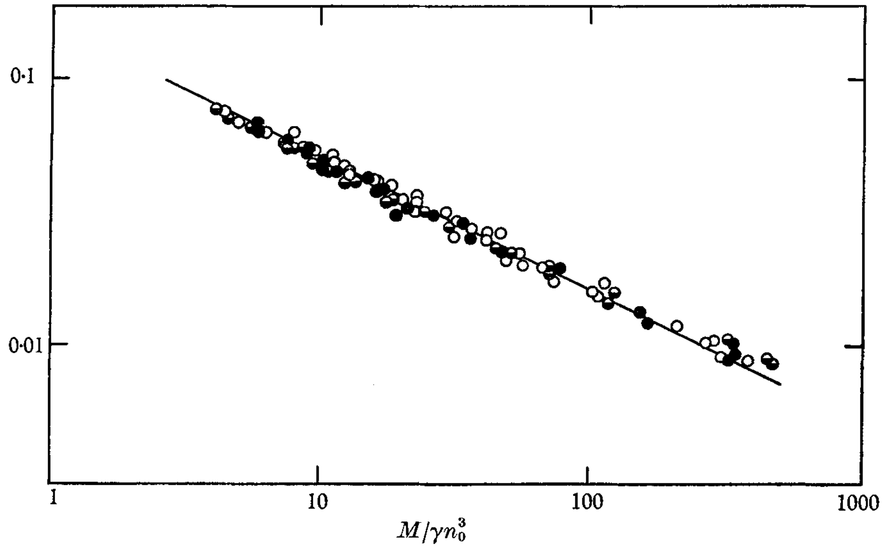

FIGURE 8. Cavity-depth data obtained in the shallow-water test apparatus using circular nozzles. Nozzle diameter: ○, $\frac{1}{4}$ in.; ◒, $\frac{1}{2}$ in.; ●, $\frac{3}{4}$ in.

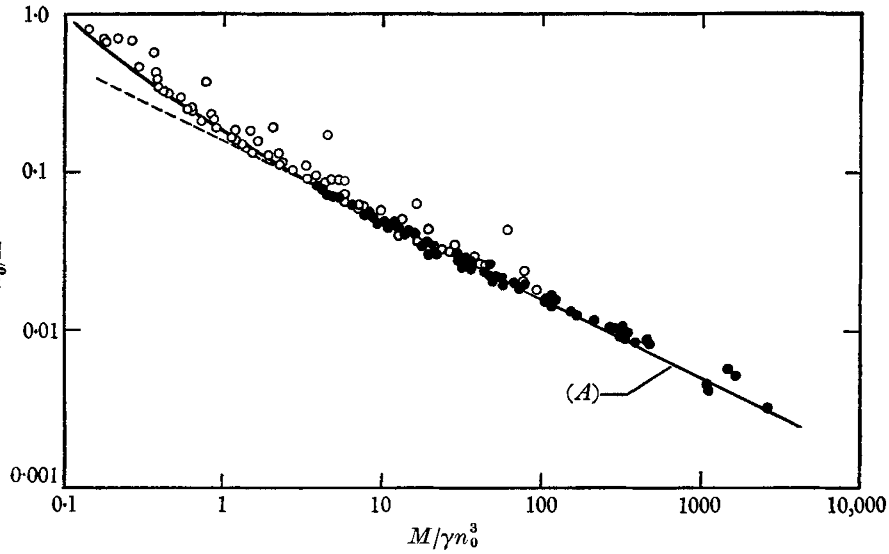

FIGURE 9. Correlation of all circular-jet cavity-depth data. ○, Deep-water tests; ●, shallow-water tests.

$$(A)\ \frac{n_0}{H} = \frac{(\pi/\beta_*)^{\frac{1}{3}}}{(M/\gamma n_0^3)^{\frac{1}{3}} - (\pi/\beta_*)^{\frac{1}{3}}}.$$

predicted fairly well by this equation. It is noticed in figure 9 that a number of points fall well above the plotted line. These points correspond to tests in which H/d_0 was less than about 8; this indicates that the jet was not behaving as a fully-developed turbulent flow. Accordingly, the data were re-plotted as shown in figure 10. The asymptote for small values of the abscissa is given by (3.11) with $\beta = 2$. An alternative form of (3.25), viz.

$$M/\gamma n_0 d_0^2 = (\pi/\beta_*)\{(H+n_0)/d_0\}^2 \tag{5.1}$$

is the asymptote for large values of $(H+n_0)/d_0$. The data appear to be compatible with these asymptotic expressions.

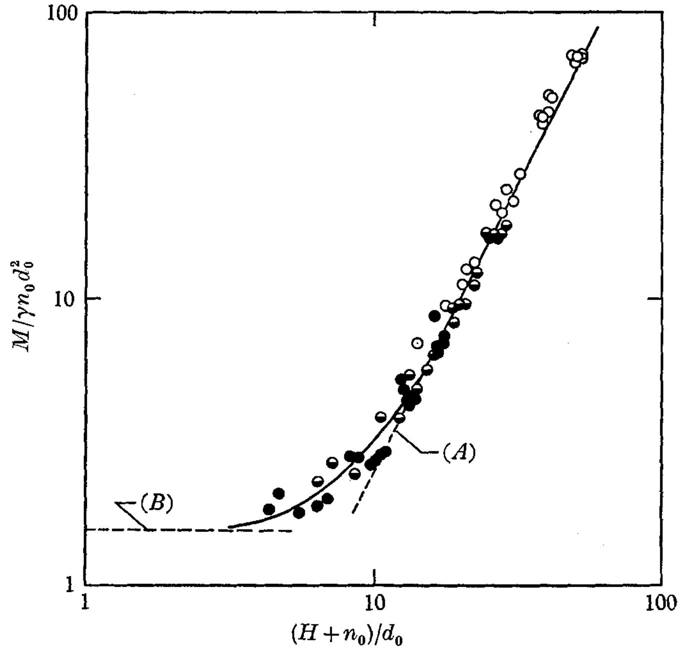

FIGURE 10. Cavity-depth data expressed in terms of the distance–diameter ratio $(H+n_0)/d_0$. Nozzle diameter: ○, $\frac{1}{4}$ in.; ◒, $\frac{1}{2}$ in.; ●, $\frac{3}{4}$ in.

$$(A)\ \frac{M}{\gamma n_0 d_0^2} = \frac{\pi}{\beta_*}\left\{\frac{H+n_0}{d_0}\right\}^2; \quad (B)\ \frac{M}{\gamma n_0 d_0^2} = \frac{\pi}{\beta} \quad (\beta = 2,\ \beta_* = 125).$$

Data were also computed in terms of the surface tension analysis of § 3.4. A value of $\sigma = 0{\cdot}005$ lb./ft. was employed in the computation. The results are shown in figure 11. This plot is similar to figure 7 except that the points now fall somewhat closer to the straight line for large values of n_0/H. However, until more data are available to examine the effect of surface tension more closely, it will be assumed that the correlations of figures 9 or 10 give the cavity depth for circular jets.

A cubic equation arises from (3.25) when an explicit solution is sought for n_0. However, for $n_0/H < 0{\cdot}1$,

$$n_0 = (\beta_*/\pi)(M/\gamma H^2), \tag{5.2}$$

where $\beta_* = 125$. Previously, Collins & Lubanska (1954) conducted experiments on the depression of a water surface by an air jet. Their results yielded a value of $\beta_* = 166$. The experiments of Poreh & Cermak gave $\beta_* = 125$ which is for-

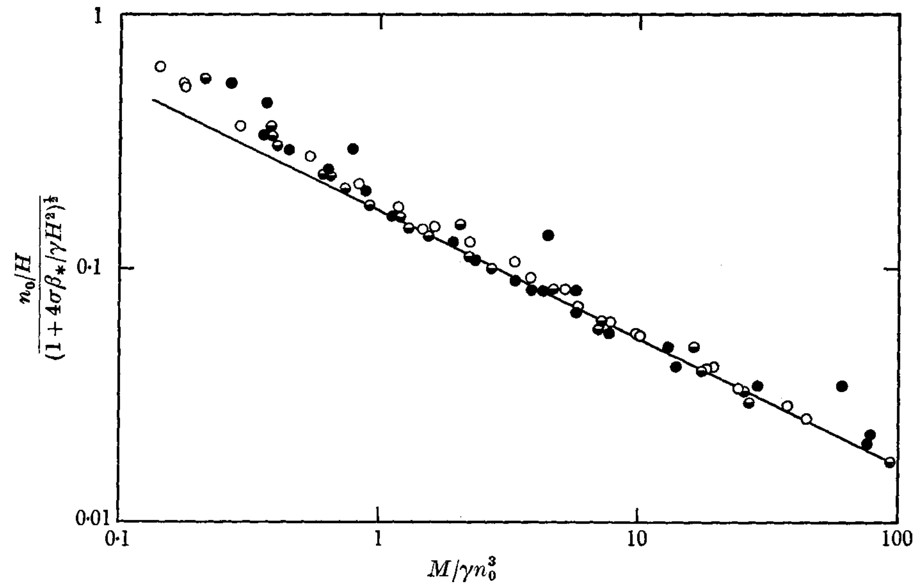

FIGURE 11. Cavity-depth data expressed in terms of the surface-tension model of (3.24). Nozzle diameter; ○, $\frac{1}{4}$ in.; ◒, $\frac{1}{2}$ in.; ●, $\frac{3}{4}$ in.

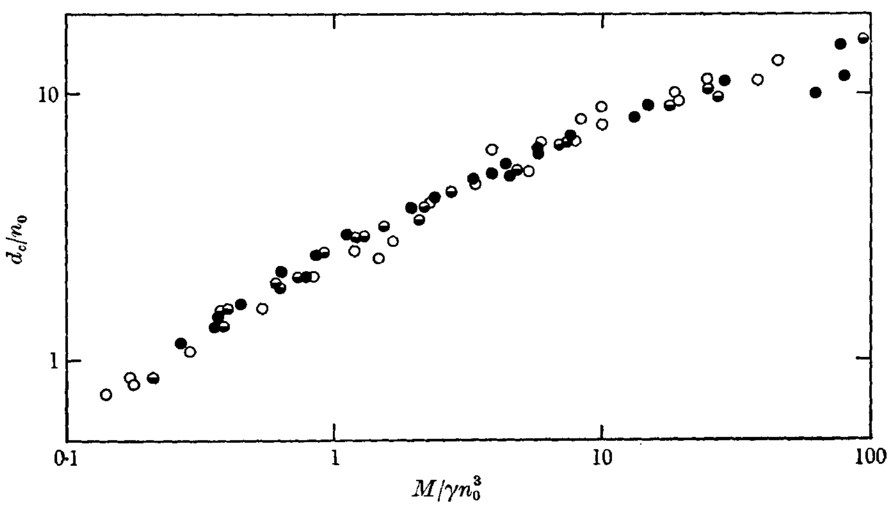

FIGURE 12. Plot of the cavity diameter-to-depth ratio. Nozzle diameter: ○, $\frac{1}{4}$ in.; ◒, $\frac{1}{2}$ in.; ●, $\frac{3}{4}$ in.

tuitously close to the result obtained in the present study. For values of n_0/H much larger than unity, (3.25) gives

$$n_0 = (\beta_* M/\pi\gamma)^{\frac{1}{3}}, \tag{5.3}$$

a result which requires considerably more data to verify. Collins & Lubanska reported values of $n_0(\gamma/M)^{\frac{1}{3}}$ in the range 3·2 to 3·8 for $H/d_0 = 0$. The average value of 3·5 is very close to that given by (5.3), viz. $(\beta_*/\pi)^{\frac{1}{3}} = 3{\cdot}42$.

A dimensionless plot of the cavity diameter is given in figure 12 and the cavity lip height is introduced in the ordinate of figure 13. A number of interpretations could be proposed for these plots. For example, figure 13 represents a 'cavity steepness ratio' relationship. From (3.15) the maximum slope of the cavity is $(2\beta_*/e)^{\frac{1}{2}}\,(n_0/H)$. Using (3.17) and assuming that this maximum slope is approximately equal to $(n_0+n_p)/\frac{1}{2}d_c$, one obtains

$$d_c/(n_0+n_p) = (2e/\pi)^{\frac{1}{2}}\,(M/\gamma n_0^3)^{\frac{1}{2}}. \tag{5.4}$$

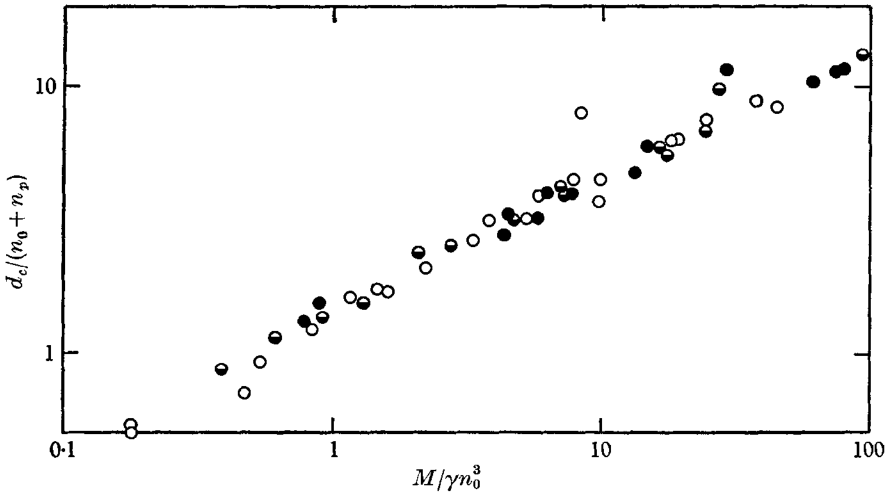

FIGURE 13. Plot of the 'cavity steepness ratio', $d_c/(n_0+n_p)$. Nozzle diameter: ○, $\frac{1}{4}$ in.; ⊖, $\frac{1}{2}$ in.; ●, $\frac{3}{4}$ in.

Figure 13 indicates that the half-power slope is predicted accurately by this analytical model though the computed curve constant is about 12 % lower than the experimental value.

When the ratio of cavity diameter to depth is small, the jet possesses an appreciable vertical velocity component following impingement. This feature may be included in an analysis by assuming the cavity to be parabolic or elliptical in form. For the circular-jet case, an assumption that the change in vertical momentum is equal to the weight of displaced liquid gives

$$M\{1+n_c'/(1+n_c'^2)^{\frac{1}{2}}\} = 2\pi\gamma\int_0^{r_c} rn\,dr, \tag{5.5}$$

where r_c defines the radius at which the gas flow separates from the liquid. It is assumed that the direction of the departing gas flow is equal to the slope of the cavity, n_c', at the separation point. If a deep parabolic cavity is selected, one obtains $d_c/n_0 = (16/\pi)^{\frac{1}{2}}\,(M/\gamma n_0^3)^{\frac{1}{2}}$ and the assumption of an elliptical cavity gives $d_c/n_0 = (12/\pi)^{\frac{1}{2}}\,(M/\gamma n_0^3)^{\frac{1}{2}}$. These results agree reasonably well with figure 12.

Over a fairly broad range, figure 12 may be described by

$$d_c/n_0 = m_2(M/\gamma n_0^3)^{\frac{1}{2}}, \tag{5.6}$$

in which the curve constant, m_2, is approximately 2·9. Utilizing (5.2), one obtains $d_c/H = m_2(\pi/\beta_*)^{\frac{1}{2}} = 0{\cdot}46$; this result is reiterated in figure 14. It is of interest to try to to express this result in terms of the velocity distribution of a free turbulent jet. The analysis of Albertson *et al.* for the circular spreading jet yields $K_2 = 1/2C_2$, where K_2 and C_2 are defined in (2.8) and (2.9), respectively. This relationship, together with the equivalence of results of (3.9) and (3.16), viz. $\beta_* = 2K_2^2$, gives

$$V/V_0 = \exp\{-\beta_*(r/x)^2\}, \tag{5.7}$$

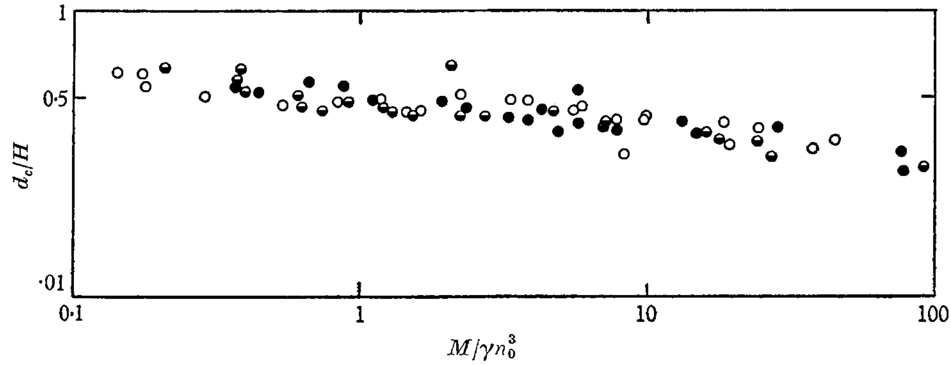

FIGURE 14. Plot of the ratio of cavity diameter to nozzle elevation. Nozzle diameter: ○, $\frac{1}{4}$ in.; ◒, $\frac{1}{2}$ in.; ●, $\frac{3}{4}$ in.

which closely resembles the assumed cavity profile equation (3.15). A fictitious velocity, V_c, is now defined as

$$V_c/V_0 = \exp\{-\beta_*(r_c/H)^2\}. \tag{5.8}$$

In other words, V_c is the velocity which the turbulent jet would have at the point (H, r_c) if the surface were absent. Since $r_c/H = \frac{1}{2}m_2(\pi/\beta_*)^{\frac{1}{2}}$, at least over a certain range, then $V_c/V_0 = \exp(-\pi m_2^2/4)$. The resulting numerical value, with $m_2 = 2{\cdot}9$, is $V_c/V_0 = 0{\cdot}0014$. Two conclusions stem from this computation. The first is that the cavity diameter is equal to about half the nozzle elevation. The second is that the cavity radius corresponds to the radius at which the jet velocity is about 0·15 % of the centre-line velocity of the associated free turbulent jet.

5.2. *Plane cavities*

Data collected from experiments using a plane nozzle in the rectangular channel are presented in figure 15. Tests in which water was moving in the channel, in a direction normal to the mid-plane of the jet, are identified by the solid points. The equation of the line passing through the open points (i.e. the still-water tests) is (3.26), with $\alpha_* = 78{\cdot}5$. The explicit solution of (3.26) yields

$$n_0/H = \tfrac{1}{2}\{(1 + 4M/k_1\gamma LH^2)^{\frac{1}{2}} - 1\}, \tag{5.9}$$

where $k_1 = (\pi/\alpha_*)^{\frac{1}{2}}$. For values of $n_0/H < 0{\cdot}1$ this reduces to

$$n_0 = (\alpha_*/\pi)^{\frac{1}{2}} M/\gamma LH, \tag{5.10}$$

and for large values of n_0/H, (5.9) becomes

$$n_0 = (M/k_1\gamma L)^{\frac{1}{2}}. \tag{5.11}$$

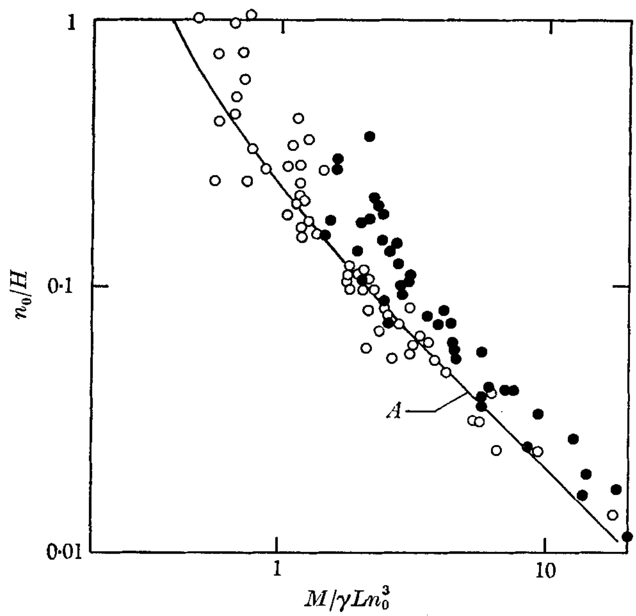

FIGURE 15. Cavity-depth area obtained in the 12 in. width open channel using a plane nozzle. ○, Still water; ●, moving water.

$$(A)\ \frac{n_0}{H} = \frac{(\pi/\alpha_*)^{\frac{1}{2}}}{(M/\gamma L n_0^3) - (\pi/\alpha_*)^{\frac{1}{2}}}.$$

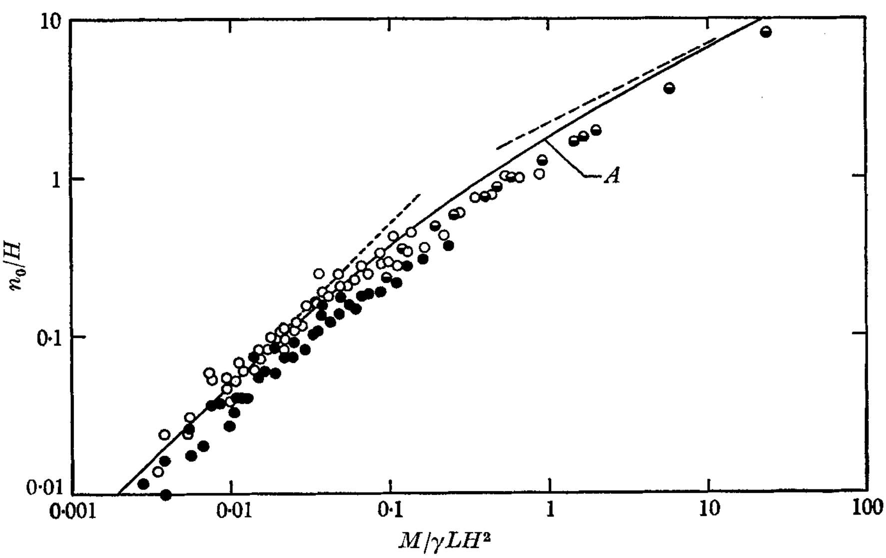

FIGURE 16. An alternative correlation of the plane-jet data, including data obtained in the 1·5 in. width open channel. ○, Still water, 12 in. channel; ●, moving water, 12 in. channel; ⊖, still water, 1·5 in. channel.

$$(A)\ n_0/H = \tfrac{1}{2}\{(1+4M/k_1\gamma LH^2)^{\frac{1}{2}} - 1\}.$$

Figure 16 presents an alternative plot of the plane-jet data; (5.9) is shown, using $\alpha_* = 78{\cdot}5$. The slope of the curve appears to be predicted correctly over the entire range but the curve constant is somewhat in error for values of n_0/H larger than about 0·2. A dimensionless plot of the cavity width is shown in figure 17. The appreciably greater scatter of the plane-jet test data was probably due to three-dimensional effects created by the channel side-walls.

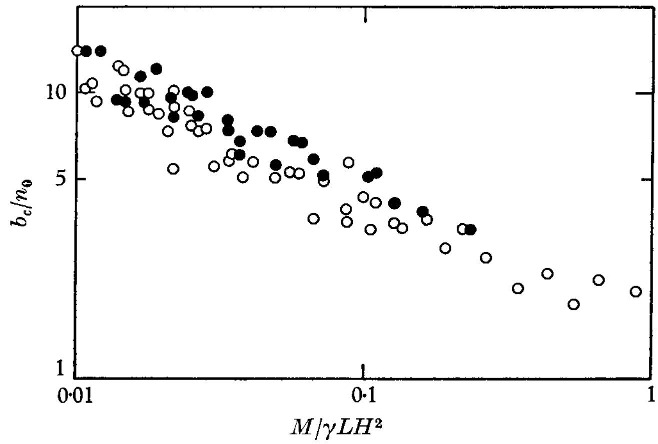

FIGURE 17. Plot of the cavity width-to-depth ratio. ○, Still water; ●, moving water.

It is apparent from figures 15, 16 and 17 that the moving-water data are distinctly separated from the still-water data. Several attempts were made to express this difference in terms of the velocity of the water. However, on the basis of these limited data, the cavity depth appears to be independent of the water velocity; the important feature seems only to be whether the water is stationary or in motion. From figure 16 it is established that the cavity depth, at least in slowly moving water ($V_L = 0{\cdot}175$ to 0·550 ft./sec), is approximately 70 % of the corresponding depth in still water. With the water in motion, the cavity became asymmetrical and the point of maximum depth was displaced downstream. It is noted that the minimum capillary wave velocity (i.e. $C_m = 0{\cdot}76$ ft./sec) exceeded the maximum water velocity in these tests, and that the maximum (Froude number)$^{\frac{1}{2}}$, $V_L/(gD)^{\frac{1}{2}}$, was 0·238. Additional work is planned for the study of plane-jet impingement on moving water.

5.3. *Sputtering*

One of the most apparent features of the phenomenon of a gas jet penetrating a liquid surface is the creation of liquid drops when the relative velocity at the interface reaches and exceeds a certain critical value. This feature is termed 'sputtering'. When the velocity of the impinging jet is small, the liquid surface is depressed slightly and the liquid at and near the surface moves radially or laterally away from the stagnation point. As a result, a circulation pattern is induced in the liquid consisting of two cylindrical vortices of opposite sense in the case of the plane jet and a toroidal vortex in the case of the circular jet. As the jet flow-rate is increased this flow pattern is more-or-less preserved, though the cavity becomes deeper. In addition, a reasonably well defined cavity lip is created. As the jet velocity is increased still further, drops begin to be thrown off into the air. It was possible to establish, with a fair degree of accuracy, when this sputtering threshold occurred. Results are given in table 5.

The criterion for sputtering is apparently established by the depth of the cavity alone. If the critical cavity depth is taken as 0·045 ft. then the centre-line velocity of the approaching air jet is approximately 50 ft./sec in the neighbourhood of the water surface. The velocity of the departing air jet would be less than this but still of the order of 40 to 50 ft./sec. Several viewpoints were taken to examine this result, though none of these shed a great deal of light. For example, the results of Schwarz & Cosart (1961) on two-dimensional wall jets indicated that the interfacial shear stress, when sputtering commenced, was about 0·031 lb./ft.^{2}. A Blasius turbulent boundary-layer computation predicted approximately 0·022 lb./ft.^{2}. The 'sheltering coefficient' analysis for wind-generated waves proposed by Jeffreys and discussed by Ursell (1956) was attempted. A rather indefinite result of this consideration was the determination of the value of the sheltering coefficient when sputtering commenced. Another viewpoint stems from the early considerations of Rayleigh (1948) regarding vibrations of a jet. For the case of an air jet penetrating through water, Rayleigh determined that the wavelength for maximum instability is $\lambda_c = 6{\cdot}48 d_0$. Thus, a critical Strouhal number $St = f_c d_0/V = d_0/\lambda_c = 0{\cdot}155$ may provide a criterion for incipient drop formation. Finally, the Kelvin–Helmholtz interfacial instability relationship was considered. This criterion predicts instability at an air–water interface when the interfacial velocity exceeds about 22 ft./sec. Considering that an instability would inherently precede the actual creation and projection of water drops, this computation is compatible with the observed sputtering velocity of about 40 to 50 ft./sec. It would be worth while to study the sputtering feature in detail using other liquids.

Apparatus	Range of cavity-depths measured in series (ft.)	Cavity-depth, in ft., when sputtering commenced		
		Mean	Min.	Max.
Deep-water series	0·010 to 0·208	0·045	0·038	0·048
Shallow-water series	0·002 to 0·067	0·045	0·039	0·052
Plane-jet series				
(a) still water	0·005 to 0·108	0·040	0·033	0·050
(b) moving water	0·005 to 0·075	0·040	0·027	0·052

TABLE 5. Sputtering threshold conditions.

5.4. *Discussion and conclusions*

A comparison of expressions obtained from the stagnation-pressure analysis and the displaced-liquid analysis resulted in the relationships $\alpha_* = \frac{1}{4}\pi K_1^4$ for the circular jet and $\beta_* = 2K_2^2$ for the plane jet. Quantities α_* and β_* are scale factors which specify the standard deviations of the cavity profiles; K_1 and K_2

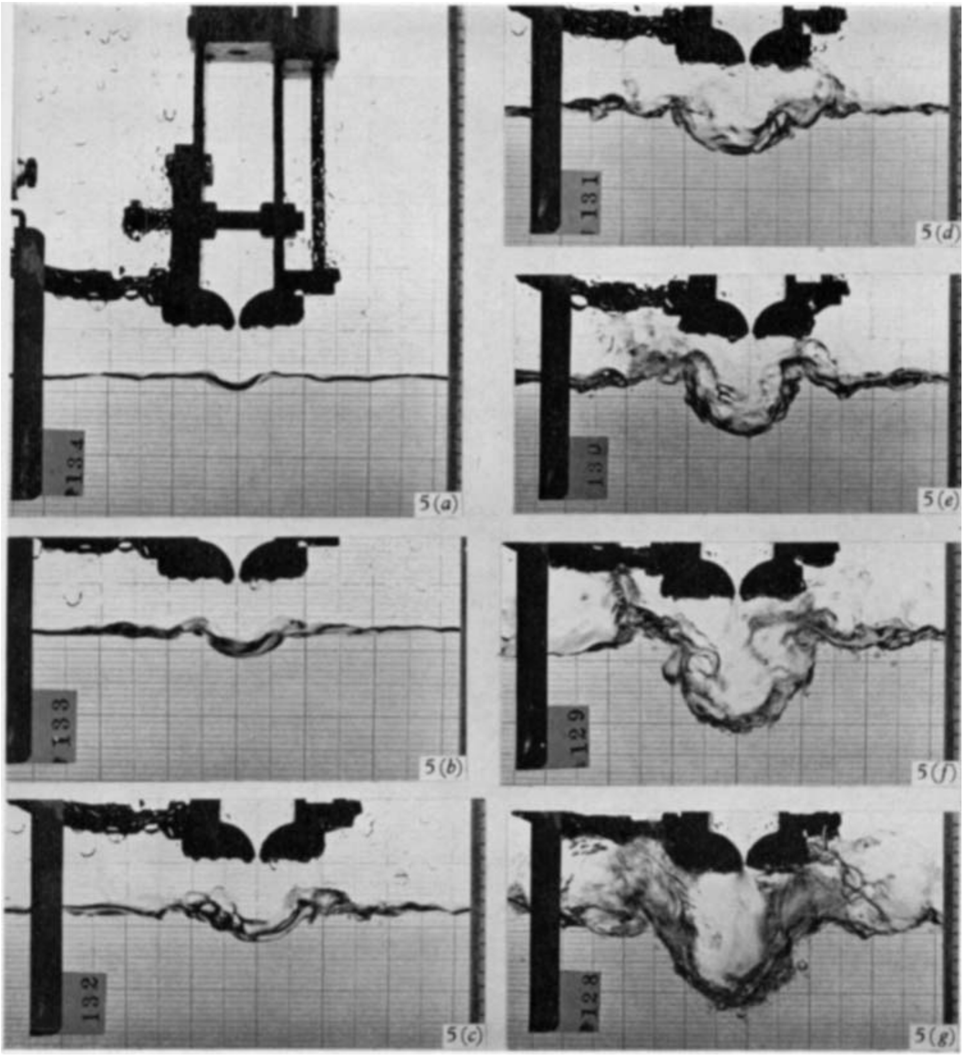

FIGURE 5. Photographs of air jet penetration into still water. Test variable is jet velocity (see table 3).

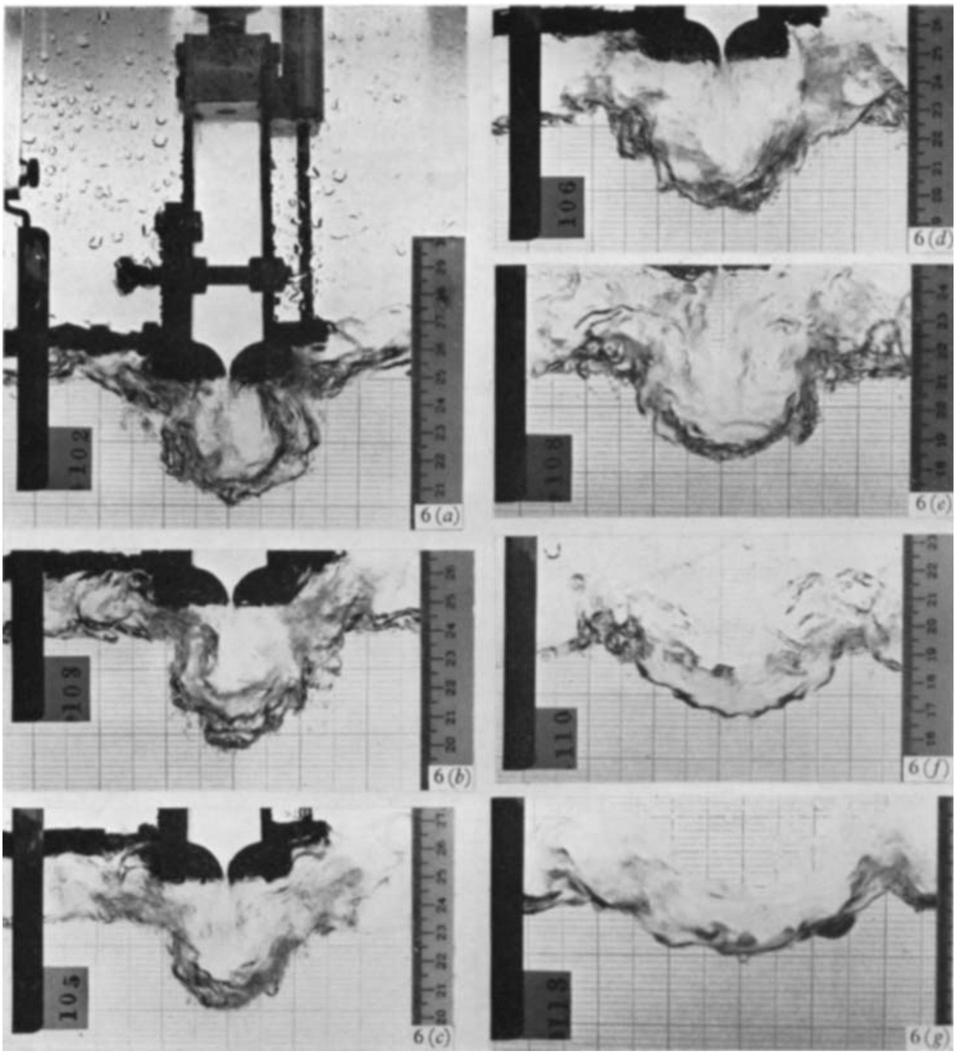

FIGURE 6. Photographs of air jet penetration into still water. Test variable is nozzle elevation (see table 4).

are constants associated with the spreading of circular and plane turbulent free jets. Values of $\alpha_* = 78{\cdot}5$ and $\beta_* = 125$ give $K_1 = 3{\cdot}17$ and $K_2 = 7{\cdot}9$. These values agree fairly well with those given in tables 1 and 2, though precise agreement is not expected since H was arbitrarily used as the value of x in the velocity distribution equations.

The quantity $1/2C_2^2$ in the circular-jet velocity-distribution equation (2.9) was replaced by β_* in (5.7); on this basis, $C_2 = 0{\cdot}063$. Townsend (1956) has presented the following equation for the circular jet

$$V/V_J = A_2(d_0/x)\,(1+\eta^2/8\beta_0)^{-2}, \tag{5.12}$$

where $\eta = r/x$ and $A_2 = (3/32\beta_0)^{\frac{1}{2}}$. Since $K_2 = A_2$, then $\beta_* = 3/16\beta_0$ and hence $\beta_0 = 0{\cdot}0015$. This compares with values of $\beta_0 = 0{\cdot}00196$ and $K_2 = 6{\cdot}39$ given by Townsend. Incidentally, matching (5.7) and (5.12) in the region of small η gives $\beta_* = 1/4\beta_0$ and hence $\beta_0 = 0{\cdot}0020$; matching at the inflexion points yields $\beta_* = 5/16\alpha_0$ and so $\beta_0 = 0{\cdot}0025$. A similar computation is made for the plane-jet case. The coefficient $1/2C_1^2$ of (2.7) is arbitrarily replaced by α_*. This yields a value of $0{\cdot}080$ for C_1. Again, Townsend gives the following expression for the plane jet

$$V/V_J = A_1(b_0/x)^{\frac{1}{2}}\,\mathrm{sech}^2\,\alpha_0\eta, \tag{5.13}$$

where $\eta = y/x$ and $A_1 = (3\alpha_0/2)^{\frac{1}{2}}$. Since $K_1 = A_1$, one obtains $\alpha_* = 9\pi\alpha_0^2/16$. This yields $\alpha_0 = 6{\cdot}6$ as compared with $\alpha_0 = 9{\cdot}1$ and $K_1 = 3{\cdot}7$ quoted by Townsend. Direct matching of arguments gives $\alpha_* = \alpha_0^2$ which results in $\alpha_0 = 8{\cdot}8$.

Though the numerical values computed above are fairly consistent, it is emphasized that this presentation is quite speculative and that considerably more evidence is needed before any rational relationships among pressure distributions, cavity profiles and the associated velocity distributions can be indicated.

Another result was obtained as a consequence of the assumptions regarding normal distribution of pressure on a surface. This result was that a free-streamline jet and a turbulent jet, impinging on a flat surface, create identical pressure distributions when $\alpha_*/\alpha = (H/b_0)^2$ for the plane jet and $\beta_*/\beta = (H/d_0)^2$ for the circular jet. However, the turbulent jet cannot exert the same stagnation pressure as the free jet does once spreading has commenced. Thus, this result offers a criterion for at least estimating the length of the potential core. Using values of $\alpha = \frac{1}{4}\pi$ and $\beta = 2$, one obtains $n_1 = H/b_0 = 10{\cdot}0$ and $n_2 = H/d_0 = 7{\cdot}9$.

The nozzle Reynolds number covered a range from 2150 to 80,000 in the test series. In this range the Reynolds number had no apparent effect on the main features of the cavity. It is concluded that the viscosity of the gas has a negligible role to play in the phenomenon beyond that normally associated with turbulent jets. However, viscous effects are undoubtedly important in connexion with interfacial instability, sputtering, and the development of circulation patterns in the liquid. Surface tension is most certainly a factor in the sputtering phenomenon and under certain conditions the cavity depth will be affected by the surface tension. The specific weight of the liquid was not varied during the tests. However, there is no doubt that γ is the all-important liquid property in the phenomenon. The same is true of the density of the gas, though again this was not varied in these tests. It is conceivable that some of the geometrical features of the test apparatus (e.g. T, D and h, shown in figure 1) could affect the test results. For example, a large value of the ratio of tank lip height, h, to tank width, T, might alter the air velocity distribution sufficiently to affect the shape of the cavity. However, over the ranges tested, these geometrical variables had no apparent effect on the results.

This investigation was carried out at Northwestern University and at the SEATO Graduate School of Engineering. The work was supported by the Bureau of Ships of the U.S. Department of the Navy under contract no. NObs-84268. Mr F. G. Collins is to be thanked for his work in collecting the shallow-water data and the co-operation of Dr A. B. Cambel is gratefully acknowledged.

REFERENCES

ALBERTSON, M. L., DAI, Y. B., JENSEN, R. A. & ROUSE, H. 1950 *Trans. Amer. Soc. Civil Engrs,* **115**, 639.

BIRKHOFF, G. 1950 *Hydrodynamics,* p. 69. Princeton University Press.

BIRKHOFF, G. & ZARANTONELLO, E. H. 1957 *Jets, Wakes and Cavities,* p. 224. New York: Academic Press.

COLLINS, R. D. & LUBANSKA, H. 1954 *Brit. J. Appl. Phys.* **5**, 22.

CORRSIN, S. & UBEROI, M. S. 1949 *NACA TN,* no. 1865.

FOLSOM, R. G. & FERGUSON, C. K. 1949 *Trans. Amer. Soc. Mech. Engrs,* **71**, 73.

FORSTALL, W. & GAYLORD, E. W. 1955 *J. Appl. Mech.* **22**, 161.

GIBSON, A. H. 1934 *Hydraulics and Its Application,* p. 372. London: Constable.

HINZE, J. O. & VAN DER HEGGE ZIJNEN, B. G. 1948 *Seventh Intern. Congr. Appl. Mech.* **2**, 286.

MILLER, D. R. & COMINGS, E. W. 1957 *J. Fluid Mech.* **3**, 1.

MILNE-THOMPSON, L. M. 1960 *Theoretical Hydrodynamics,* p. 291. London: Macmillan.

POREH, M. & CERMAK, J. E. 1959 *Proc. Sixth Midwest Conf. on Fluid Mech.,* Austin, p. 198.

RAYLEIGH, LORD 1948 *The Theory of Sound,* vol. II, p. 362. New York: Dover Publications.

REICHARDT, H. 1941 *Z. angew. Math. Mech.* **21**, 257.

SCHWARZ, W. H. & COSART, W. P. 1961 *J. Fluid Mech.* **10**, 481.

TOWNSEND, A. A. 1956 *The Structure of Turbulent Shear Flow,* p. 187. Cambridge University Press.

URSELL, F. 1956 *Surveys in Mechanics,* ed. BATCHELOR, G. K. & DAVIES, R. M., p. 225. Cambridge University Press.